Characteristics of a Silicon Nanowires/PEDOT:PSS Heterojunction and Its Effect on the Solar Cell Performance

Zhimin Liang,[†] Mingze Su,[†] Hao Wang,[‡] Yuting Gong,[§] Fangyan Xie,[§] Li Gong,[§] Hui Meng,[†] Pengyi Liu,[†] Huanjun Chen,[‡] Weiguang Xie,*,[†] and Jian Chen*,[§]

[†]Siyuan Laboratory, Department of Physics, Jinan University, Guangzhou, Guangdong 510632, P. R. China
[§]Instrumental Analysis & Research Center and [‡]State Key Lab of Optoelectronic Materials and Technologies, Sun Yat-sen University, Guangzhou 510275, P. R. China

Ⓢ Supporting Information

ABSTRACT: The interfacial energy-level alignment of a silicon nanowires (SiNWs)/PEDOT:PSS heterojunction is investigated using Kelvin probe force microscopy. The potential difference and electrical distribution in the junction are systematically revealed. When the PEDOT:PSS layer is covered at the bottom of the SiNW array, an abrupt junction is formed at the interface whose characteristics are mainly determined by the uniformly doped Si bulk. When the PEDOT:PSS layer is covered on the top, a hyperabrupt junction localized at the top of the SiNWs forms, and this characteristic depends on the surface properties of the SiNWs. Because the calculation shows that the absorption of light from the SiNWs and the Si bulk are equally important, the bottom-coverage structure leads to better position matching between the depletion and absorption area and therefore shows better photovoltaic performance. The dependence of J_{SC} and V_{OC} on the junction characteristic is discussed.

KEYWORDS: solar cell, heterojunction, coverage effect, silicon nanowires, cross-sectional imaging, built-in potential
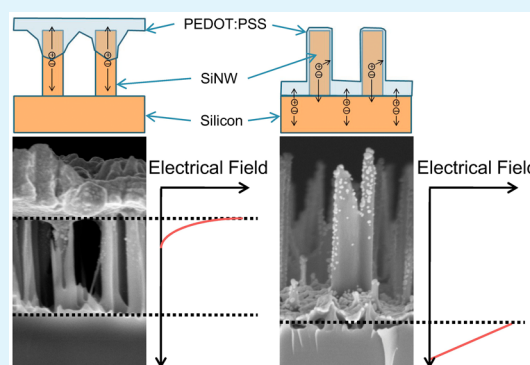
1. INTRODUCTION

The silicon/organic hybrid solar cells have gained considerable interest in recent years because they take advantage of the superior electrical properties of silicon and the low-cost processing of the organic materials.[1−4] The core−shell structure of a silicon nanowires (SiNWs)/organic hybrid solar cell has been considered to have high light absorption and fast electron/hole pair separation and carrier collection.[5−7] The merit of the structures can only be realized by surface passivation, such as for SiO_x,[8] AlO_x,[9,10] $−CH_3$,[11,12] and other interfacial layers.[13,14] The trap density at the interface will be significantly reduced by surface passivation, resulting in a high minority carrier lifetime and thus raising the power conversion efficiency (PCE) of the devices. The interfacial energy alignment is another key factor that determines the PCE. Yu et al. found that although the 1,1-bis[(di-4-tolylamino)phenyl]-cyclohexane (TAPC) layer covering the SiNW array showed a lower minority lifetime than that of the unmodified SiNW array, the TAPC-modified device shows higher PCE. A better heterojunction band offset at the TAPC-modified interface was suggested to mitigate the interface recombination.[13] Besides, a high built-in potential, which affects the value of V_{OC}, also depends on careful control of the interfacial alignment. A traditional Schottky-like model has been frequently adopted for analysis of the carrier transfer behavior.[15−18] Under this

assumption, Avasthi et al. suggested that a highly efficient cell should have low energy offset between E_{VSi} and the highest occupied molecular orbital (HOMO) and high energy offset between E_{CSi} and the lowest unoccupied molecular orbital (LUMO).[15] Zhang et al. showed that the SiNWs/PEDOT:PSS device with an ideal factor closer to 1 showed the better performance. However, a higher ideal factor was normally observed; for example, a value of 2.83 was found in a device fabricated with SiNWs with a length of 7.80 μm.[16] Although meaningful results have been derived, the studies show that deviation from the model is popular and its origin is not understood. The interfacial nature of a SiNWs/organic hybrid junction is still not revealed directly from experiment.

It is found that the length and density of the SiNWs strongly affect the PCE of the solar cell.[9,16,17] We found that, with different lengths and densities, two types of coverage were always observed in a SiNWs/PEDOT:PSS hybrid solar cell: one with a PEDOT:PSS layer on top of the SiNWs (Figure 1a) and one with a PEDOT:PSS layer immersed in the bottom of the SiNWs (Figure 1b). In this study, we systematically measure the surface potential distribution along the junction area using
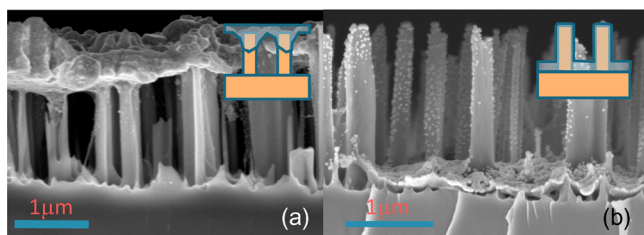
Figure 1. SEM images of a PEDOT:PSS-coated SiNW array. (a) Device T: top coverage. (b) Device B: bottom coverage.

Kelvin probe force microscopy (KPFM). The interfacial energy-level alignment and the electrical field distribution in the junction were revealed. Combined with the theoretical calculation of the absorption distribution, we discuss the mechanism that induced the PCE difference in the two types of devices.

2. RESULTS AND DISCUSSION

2.1. Potential and Electrical Field Distribution in a SiNWs/PEDOT:PSS Heterojunction. Two types of devices are prepared and shown in Figure 1. In Figure 1a, the PEDOT:PSS layer was coated at a low spin speed of 2000 rpm. The scanning electron microscopy (SEM) image shows that the PEDOT:PSS layer was mainly coated on top of the SiNWs. Part of PEDOT:PSS permeated along the surface of the SiNWs into the inside, but the root of the SiNWs was not covered. The main interface was located at the top of the SiNW array (named as device T hereafter). In Figure 1b, the PEDOT:PSS layer was

coated at a higher spin speed of 4000 rpm. Maybe because of the smaller thickness, the SEM image shows that PEDOT:PSS fully penetrated into the space among the SiNWs and covered the SiNWs and its bottom. A large interface located at the root of the SiNW array is observed (named as device B hereafter).

The surface potential images (Figure S1b,c in the Supporting Information, SI) along the cross section of both devices were revealed using KPFM, and typical profiles are shown in Figure 2a,b. It is shown that the surface potential dropped sharply at the area where the organic/inorganic junction formed. The initial potential differences at the junctions were around 0.85 eV in both devices. This shows that, in equilibrium condition, the Fermi level of the Si (4.25 eV) is aligned to the HOMO of PEDOT:PSS (around 5.0−5.2 eV)[19,20] regardless of the structure. This indicates that the junctions were well formed in both devices. The measured built-in potential is higher than those (around 0.6 eV) calculated from the diode model.[16,21] This is because the junction is not an ideal pn junction, as will be discussed below.

By differentiation of the potential distribution along the surface normal, the electrical field distribution can be calculated and is shown in Figure 2c,d. They clearly show where the depletion areas resided in both devices. In device T, the electrical field mainly dropped on the nanowires. The maximum electrical field is about 0.34 V/μm, which is close to the electrical field in a Si pn junction. In device B, the maximum initial electrical field is close to the value in device T, while the field locates near the bottom of the SiNWs and extends into the bulk.
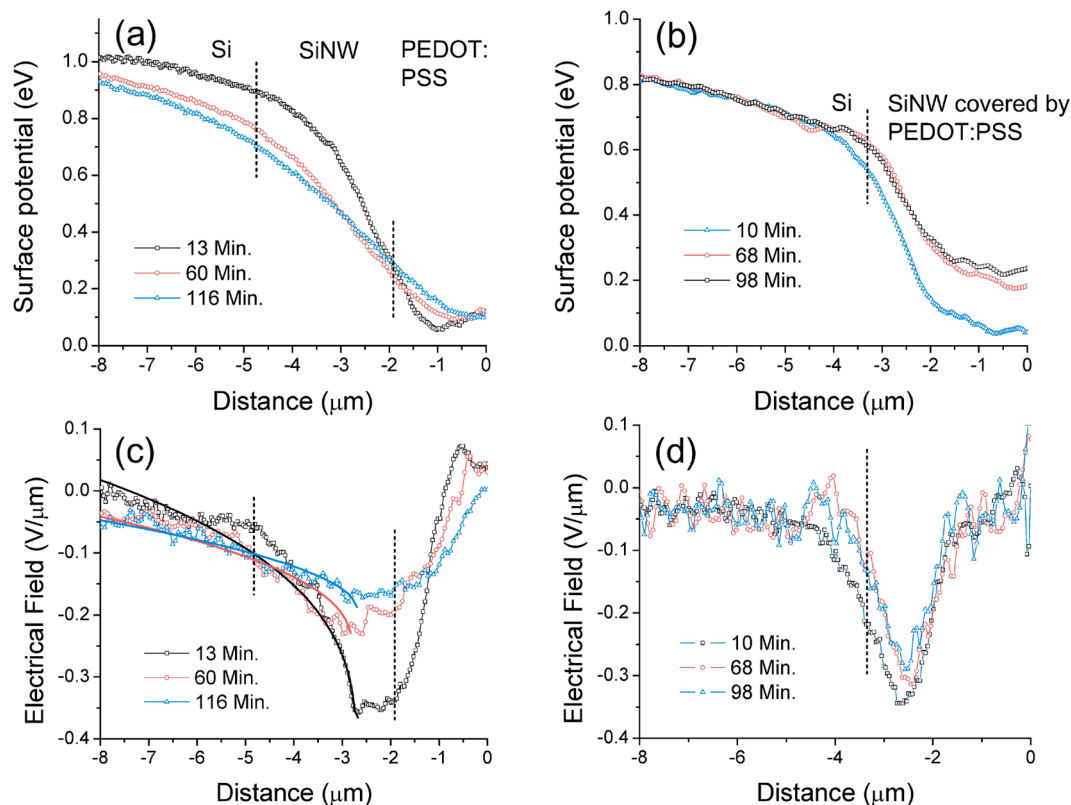

Figure 2. (a and b) Time-dependent surface potential distribution along the junctions in devices T and B, respectively. (c and d) Corresponding electrical field distribution along the junction calculated from parts a and b, respectively. The dashed lines roughly mark the location of the contact interface.
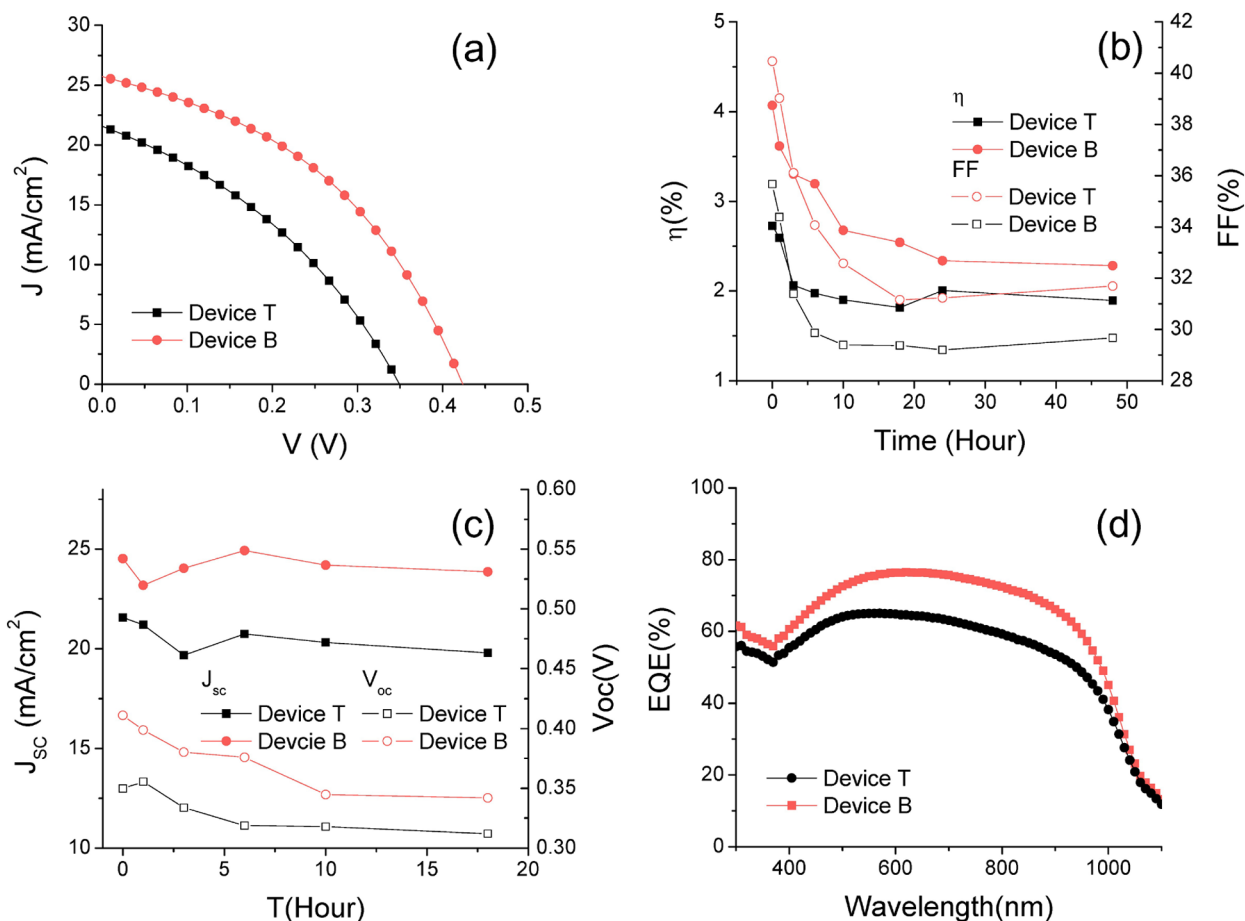
Figure 3. (a) IV characteristics of the two devices. (b) η and FF of the devices. (c) J_{SC} and V_{OC} of the device. (d) EQE spectra of the two devices.

Time-dependent surface potential measurements in Figure 2a,b show that in device T the surface potential of SiNWs decreases and that of PEDOT:PSS increases as the air exposure time increases. It is found that the surface potential of PEDOT:PSS near the device surface (distance = 0 in Figure 2) remains constant, which means that PEDOT:PSS is unlikely to be affected by the air in this time period. This is consistent with the IV measurement that the conductance of PEDOT:PSS is not changed in air in our experiment and in another reference.[2] The change of the surface potential started from the interface and extended toward both sides as time went away. This suggests that traps were first formed at the interface, which can be attributed to the formation of a Si–SiO$_x$ surface layer on the SiNWs because it can trap both electrons and holes. As the traps formed on the surface of SiNWs, it strongly affected the surface potential of PEDOT:PSS in device B. The trapping of holes raised its surface potential and reduced the apparent potential difference to 0.65 eV after 98 min of exposure.

The strength of the electrical field in the depletion area decreased in both devices. In device B, the electrical field reduced to 0.29 V/μm upon 98 min of air exposure. It is found that the shape of the electrical field distribution remains the same during the measurement period. It could be well fitted by a linear function, which means that this organic/inorganic junction can be described by the classical abrupt junction model. It can be understood that the junction mainly forms between the bulk Si and the PEDOT:PSS layer.

In device T, the maximum electrical field reduced sharply to 0.17 V/mm in 116 min of exposure. At the same time, the

shape of the depletion area was found to change greatly and extend into the bulk. The pn junction is modeled using the Poisson equation:[22]

$$\frac{d^2\Psi}{dx^2} = \frac{dE}{dx} = -\frac{\rho(x)}{\varepsilon_s \varepsilon_0} = -B\left(\frac{x}{x_0}\right)^m \tag{1}$$

where Ψ is the potential difference, E is the electrical field, and ε_s and ε_0 are the dielectric constants of the semiconductor and vacuum. B is a constant depending on the doping concentration, and x_0 is the position of the interface between n- and p-type areas. m is a constant that describes the type of pn junction. For an abrupt junction, the m value is equal to 0. For a linearly graded junction, m is equal to 1. A hyperabrupt junction has a negative m value, in which the charge concentration is rapidly reduced as the distance from the junction interface increases. It can be seen that the electrical field can be described by a power function. Therefore, we fit the electrical field distribution at the Si side using a power function:

$$E = E_0 + A(x - x_0)^P \tag{2}$$

where E_0 is the electrical field far away from the interface, A is a constant dependent on the charge concentration in the depletion, and $P - 1$ is a constant equal to m in eq 1. The fitting parameters are given in Table S1 in the SI. We found that P of the SiNWs/PEDOT:PSS junction is smaller than 1, so $P - 1$ is negative. This means that the junction is similar to a hyperabrupt junction in which the charge density at the very interface is much higher and decays rapidly. It has been found

that surface passivation of Si–CH$_3$ led to a strong surface dipole that can bend up the surface energy level by 0.37 eV.[23] Therefore, we attribute the formation of a hyperabrupt junction to surface passivation on the SiNWs.

2.2. Performance of a SiNWs/PEDOT:PSS Heterojunction. Typical performances of the devices are shown in Figure 3. Device T showed an open-circuit voltage (V_{OC}) of 0.35 V, a short-circuit current density (J_{SC}) of 21.5 mA/cm^2, and a fill factor (FF) of 35.62%, giving a PCE of 2.7%. In device B, a better PCE of 4.0% with V_{OC} of 0.42 V, J_{SC} of 24.5 mA/cm^2, and FF of 41.22% was observed. The stabilities of the devices were also measured and are shown in Figure 3. Although the PCE of both devices decayed obviously, the PCE of device B remained 2.5% after 18 h of storage in air conditioning, while the PCE of device T was 1.8%. Comprehensive studies on devices from different chips (Figure S2 in the SI) show the same tendency, giving support that the coverage effect has universality.

In the SEM image in Figure 1, we can see that the silver coverage in device B is not continuous near the top of the SiNWs, which means that its carrier collection by electrode may be less efficient than that in device T. However, external quantum efficiency (EQE) measurements in Figure 3d show that device B has a higher EQE than device T. Because the two devices were fabricated in one single chip, the difference should come from the device architecture and junction characteristics. It is clearly found that, although the electrical fields in both devices decrease greatly, the decay of J_{SC} was not obvious during this period. A dramatic J_{SC} drop was observed only several days later in both types of devices (Figure S2 in the SI). Therefore, the electrical field and potential difference in the junction area are enough for full separation of the carriers as long as the carriers can reach the depletion region. Therefore, we consider that diffusion of the electron–hole pair to the depletion area may be the key difference.

2.3. Mechanism of the Coverage Effect. Compared to a bare Si surface, SiNWs are expected to have much better light-trapping properties, which enhance the absorption of light.[5] Figure 4a shows a calculated absorption distribution along the SiNWs at a light of 555 nm. A stronger power dissipation density is observed along the entire SiNW. The power dissipation density of the Si substrate is around 1/20 of the
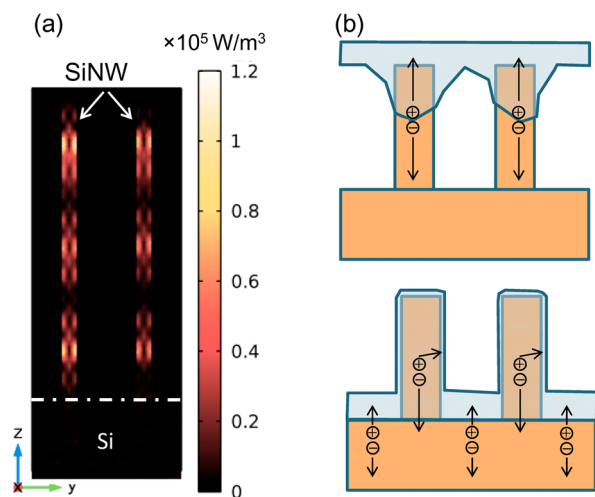

Figure 4. (a) Power dissipation density distribution in the SiNW array. (b) Schematic of electron–hole pair separation in the devices.

value at the top of the SiNWs. However, because of the limited density and length of the SiNWs, the SiNW array cannot absorb all of the energy of light. We found that the total absorption of SiNWs is 1.179×10^{-15} W in a unit cell, which is close to the substrate absorption of 9.641×10^{-16} W. The results show that absorptions from the Si substrate and the SiNW array are equally important. This inference is consistent with former studies indicating that PCE will decrease when the thickness of the Si substrate is lower than 10 μm.[24] Therefore, an optimum hybrid junction is suggested to efficiently separate the electron–hole pair and collect holes generated from both the substrate and SiNWs.

The prerequisite of efficient electron–hole pair separation is determined by whether the carrier can diffuse into the depletion area. The carrier diffusion length of SiNWs is determined by the surface trap. Although the carrier diffusion length of Si bulk is tens of micrometers, scanning photocurrent microscopy experiments show that the diffusion length of SiNW may decrease to about 2 μm.[25] It is found in our experiment and in work by other research groups that the optimized SiNW length for the hybrid solar cell is in the range of 0.4–2.1 μm, so the diffusion length of the as-prepared SiNW is expected to have the same order.[9,16] Considering device T with the depletion layer near the top of the SiNWs, hole carriers from the bulk are not easy to diffuse across the bulk and the SiNWs to the depletion layer near the top of the SiNWs, leading to low collection efficiency of holes (Figure 4b). In device B, the depletion layer locates at the bottom of the SiNWs, and the carrier separation and collection from the SiNWs and the bulk are more efficient. Therefore, we can conclude that the superior performance of device B comes from the better position matching of the absorption and depletion areas. One of the inferences of the mechanism is the length-dependent PCE, as has been observed in studies.[9,16] We also fabricate a top-coverage device with a SiNW length of about 500 nm. The depletion area will locate closer to the Si bulk; therefore, a larger PCE close to the bottom-coverage one (Figure S4 in the SI) is observed.

2.4. V_{OC} of the SiNWs/PEDOT:PSS Heterojunction. The decrease of the PCE in both devices is caused by the dramatic drop of FF as well as V_{OC}. It is not easy to discuss the junction effect on FF because it depends on many factors of the devices. However, the maximum V_{OC} depends on the interfacial energy-level alignment. The energy-level alignment at the interface is constructed according to the surface potential profile in Figure 2 and shown in Figure 5b. Compared with the vacuum-level-aligned energy diagram in Figure 5a, the maximum value of V_{OC} is dependent on three parameters. (1) The built-in potential difference of the junction. This determines the external voltage to reach flat band. (2) The energy difference between E_C and LUMO in Figure 5b that determines the electron barriers from Si to PEDOT:PSS. (3) The energy difference between E_V and HOMO in Figure 5b that determines the hole barriers from PEDOT:PSS to Si. In Figure 5b, the built-in potential difference of the junction (ΔE_{bi}), which is equal to $E_{FSi} - E_{HOMO}$ in Figure 5a, will determine V_{OC} because it is the smallest energy offset of the above three values. However, V_{OC} is always smaller than this one. Because surface dipoles always exist at the surface of Si, flat band condition cannot be realized because the HOMO will be pinned by the surface states. Therefore, V_{OC} is determined by $E_F - E_{HOMO} - \Delta E_S$, where ΔE_S is the surface band bending of Si caused by the surface defects. Surface passivation by –CH$_3$ leads to a maximum
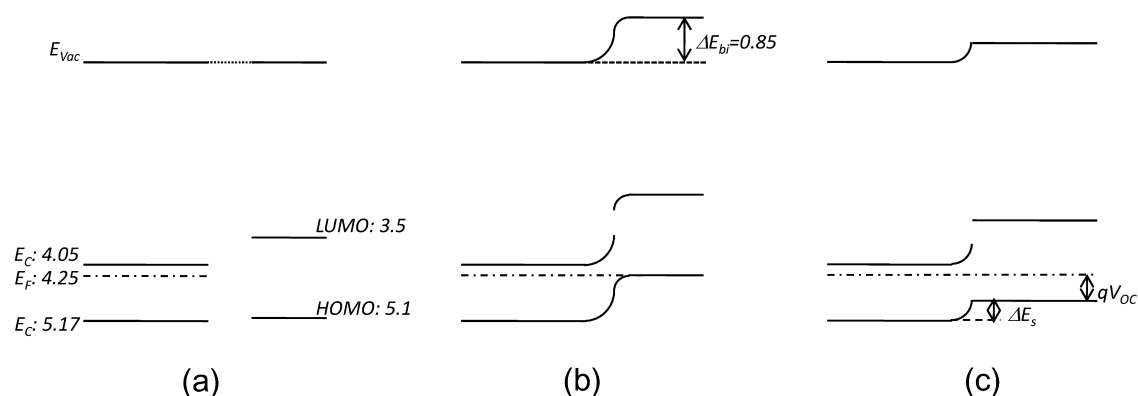
Figure 5. (a) Energy level of Si and PEDOT:PSS under vacuum-level alignment. (b) Equilibrium energy-level alignment according to the KPFM results. (c) Energy-level alignment under illumination that gives a maximum V_{OC}. The units of the values is electronvolts.

surface band bending of 0.37 eV.[23] Therefore, V_{OC} of 0.48 eV is expected, which is close to the maximum value observed in our experiments (Figure S2 in the SI). The results indicate two ways to raise the V_{OC} values. The first is to use Si with higher E_F or PEDOT:PSS with lower HOMO. However, it is shown that the work function of PEDOT:PSS increases as the conductivity decreases.[26−28] Therefore, there should be a consideration of balance. The second is to reduce the energy band bending after surface passivation. Long or dense SiNWs lead to increasing band bending at the interface of the junction because the trap density will increase; therefore, a decrease of V_{OC} is always observed.[9,16,17] The formation of a junction to the bulk Si reduces the defect effect from the SiNWs, so bigger V_{OC} is observed in device B. Precise control of the SiO_x surface layer gives a small surface band bending of 0.15 eV; therefore, an optimized V_{OC} as high as 0.6 eV can be observed.[8]

3. CONCLUSION

The SiNWs/PEDOT:PSS junction characteristic was systematically revealed. The junction can be a classical abrupt junction or a hyperabrupt junction depending on the coverage status of the PEDOT:PSS layer. A built-in potential difference of 0.85 eV is found, while V_{OC} depends on the surface band bending by the surface dipoles. The electrical field in the junction is normally high enough to separate and collect carriers so J_{SC} is normally unchanged at the initial hours. Absorptions from the SiNWs and Si substrate are both important in the SiNWs/PEDOT:PSS solar cell. The position matching between the junction and absorption area is the key factor for a highly efficient SiNWs/PEDOT:PSS solar cell, which determines that bottom-coverage devices have superior performance over top-coverage ones. The findings show a clear picture of the SiNWs/PEDOT:PSS junction, which will help to improve the performance of the hybrid solar cell.

4. EXPERIMENTAL SECTION

4.1. Preprocessing of Si. The n-type (100) Si wafer with a resistivity of 1−3 Ω·cm was ultrasonically cleaned in acetone, ethanol, and deionized water in sequence for 15 min, respectively. The substrate was then cleaned with a piranha solution (3:1 H_2SO_4/H_2O_2) at 80 °C for 30 min and rinsed with deionized water several times. Finally, the sample was dried by a stream of N_2.

4.2. Growth of the SiNW Array. The SiNW array was produced on the Si wafer by metal-assisted chemical etching.[29] In detail, the Si substrate was immersed in a solution consisting of 4.8 M hydrofluoric acid (HF) and 0.02 M silver nitrate ($AgNO_3$) at 50 °C. The length of the SiNWs was controlled by the etching time. Then the substrate was

cleaned with deionized water and dipped into a HNO_3 solution (30% w/w) for 30 min to completely remove all of the residual silver between each nanowire. Finally, the SiNW array was cleaned with deionized water and dried with N_2.

4.3. CH₃-Terminated SiNW Array Preparation. The two-step chlorination/alkylation process was used to fabricate the methyl-terminated SiNW array.[30] The H-terminated SiNW array were obtained by immersing the SiNW array into a HF solution (5 M) for 10 min. Then the H-terminated SiNW array was cleaned with deionized water and dried under a stream of N_2. The sample was then transferred into a glovebox quickly. The sample was immersed in an aqueous solution of superfluous phosphorus pentachloride (PCl_5) in chlorobenzene (CB) at 100 °C for 2 h. After this process was finished, the sample was cleaned with CB three times and immersed in tetrahydrofuran (THF) for several minutes, and then the SiNW array substrate was immersed in a solution of CH_3MgCl (1 M) in THF for 8 h at 80 °C. The methyl-terminated SiNW array was formed after the sample was rinsed with THF and immersed in methyl alcohol for 20 min.

4.4. Fabrication of the SiNW Array Hybrid Solar Cell. Aluminum of 200 nm thickness was deposited on the back side of the sample as a rear electrode by thermal evaporation. Highly conductive PEDOT:PSS (Clevios PH 1000) uniformly mixed with 5 wt % dimethyl sulfoxide and 1 wt % Triton X-100 was spin-coated onto the surface of the CH_3-terminated SiNW array in air. Following that, the sample was annealed at 140 °C for 10 min in air. The conductivity of the as-prepared thin film is around 10^2 S/cm.[31] Silver grids of 100 nm thickness were deposited on the surface of PEDOT:PSS by thermal evaporation as the top electrode through a shadow mask.

4.5. Device Characterization. A Keithley 2400 sourcemeter was used to measure the photovoltaic current density−voltage characteristics of all of the devices under 100 mW/cm² AM 1.5G illumination using a SUN 2000 solar simulator (Abet Technologies). The EQE of the device was measured with Enlitech's QE-R system. The structure of the SiNW was characterized by a Zeiss Ultra 55 scanning electron microscope. The surface morphology and surface potential of the junction were characterized using a Bruker Dimension Icon atomic force microscope in air in KPFM mode. The bright contrast in the surface potential image means higher surface potential but lower vacuum level and vice versa.[32,33] Details on the cross-sectional imaging can be found in the SI.

4.6. Numerical Calculations. Numerical calculations were conducted using a finite-element method (COMSOL, version 4.3b) in the frequency domain. The dielectric function of Si was taken according to previously reported values.[34] The SiNW array was modeled as periodic Si cylinders adhered to the Si substrate. The calculations were performed in a unit cell, while periodic boundary conditions were applied to model the array structure. The thickness of the substrate was set to 500 nm, the diameter of the Si cylinder was 100 nm, and the length of the nanowire was 2 μm. The lattice constant

was 500 nm. The refractive index of the surrounding medium was set as 1.0. The incident light was modeled using a plane wave launching normal to the surface. Fine meshes were used for the nanostructures and surroundings.

■ ASSOCIATED CONTENT

⑤ Supporting Information

Schematic setup of KPFM cross-sectional measurement and images (Figure S1), long-term measurement of the device performance (Figure S2), power dissipation density along the center of a nanowire (Figure S3), performance of the top-coverage SiNWs/PEDOT:PSS solar cell fabricated with a SiNW length of around 500 nm (Figure S4), and fitting parameters using eq 2 (Table S1). This material is available free of charge via the Internet at http://pubs.acs.org.

■ AUTHOR INFORMATION

Corresponding Authors

*E-mail: wgxie@jnu.edu.cn.
*E-mail: puscj@mail.sysu.edu.cn.

Notes

The authors declare no competing financial interest.

■ ACKNOWLEDGMENTS

■ REFERENCES

(1) Liu, C.-Y.; Holman, Z. C.; Kortshagen, U. R. Hybrid Solar Cells from P3HT and Silicon Nanocrystals. *Nano Lett.* **2008**, *9*, 449−452.

(2) He, W. W.; Wu, K. J.; Wang, K.; Shi, T. F.; Wu, L.; Li, S. X.; Teng, D. Y.; Ye, C. H. Towards Stable Silicon Nanoarray Hybrid Solar Cells. *Sci. Rep.* **2014**, *4*, 1−7.

(3) Song, T.; Lee, S.-T.; Sun, B. Silicon Nanowires for Photovoltaic Applications: The Progress and Challenge. *Nano Energy* **2012**, *1*, 654−673.

(4) Kulakci, M.; Es, F.; Ozdemir, B.; Unalan, H. E.; Turan, R. Application of Si Nanowires Fabricated by Metal-Assisted Etching to Crystalline Si Solar Cells. *IEEE J. Photovoltaics* **2013**, *3*, 548−553.

(5) Garnett, E.; Yang, P. Light Trapping in Silicon Nanowire Solar Cells. *Nano Lett.* **2010**, *10*, 1082−1087.

(6) He, L.; Jiang, C.; Rusli; Lai, D.; Wang, H. Highly Efficient Si-Nanorods/Organic Hybrid Core−Sheath Heterojunction Solar Cells. *Appl. Phys. Lett.* **2011**, *99*, 021104.

(7) Wang, K. X.; Yu, Z.; Liu, V.; Cui, Y.; Fan, S. Absorption Enhancement in Ultrathin Crystalline Silicon Solar Cells with Antireflection and Light-Trapping Nanocone Gratings. *Nano Lett.* **2012**, *12*, 1616−1619.

(8) He, L.; Jiang, C.; Wang, H.; Lai, D. Rusli; High Efficiency Planar Si/Organic Heterojunction Hybrid Solar Cells. *Appl. Phys. Lett.* **2012**, *100*, 073503.

(9) Pudasaini, P. R.; Ruiz-Zepeda, F.; Sharma, M.; Elam, D.; Ponce, A.; Ayon, A. A. High Efficiency Hybrid Silicon Nanopillar−Polymer Solar Cells. *ACS Appl. Mater. Interfaces* **2013**, *5*, 9620−9627.

(10) Erickson, A. S.; Kedem, N. K.; Haj-Yahia, A. E.; Cahen, D. Aluminum Oxide−n-Si Field Effect Inversion Layer Solar Cells with Organic Top Contact. *Appl. Phys. Lett.* **2012**, *101*, 233901.

(11) Zhang, F. T.; Sun, B. Q.; Song, T.; Zhu, X. L.; Lee, S. Air Stable, Efficient Hybrid Photovoltaic Devices Based on Poly(3-hexylthiophene) and Silicon Nanostructures. *Chem. Mater.* **2011**, *23*, 2084−2090.

(12) Haick, H.; Hurley, P. T.; Hochbaum, A. I.; Yang, P. D.; Lewis, N. S. Electrical Characteristics and Chemical Stability of Non-oxidized, Methyl-terminated Silicon Nanowires. *J. Am. Chem. Soc.* **2006**, *128*, 8990−8991.

(13) Yu, P.; Tsai, C.-Y.; Chang, J.-K.; Lai, C.-C.; Chen, P.-H.; Lai, Y.-C.; Tsai, P.-T.; Li, M.-C.; Pan, H.-T.; Huang, Y.-Y.; Wu, C.-I.; Chueh, Y.-L.; Chen, S.-W.; Du, C.-H.; Horng, S.-F.; Meng, H.-F. 13% Efficiency Hybrid Organic/Silicon-Nanowire Heterojunction Solar Cell via Interface Engineering. *ACS Nano* **2013**, *7*, 10780−10787.

(14) Bashouti, M. Y.; Sardashti, K.; Schmitt, S. W.; Pietsch, M.; Ristein, J.; Haick, H.; Christiansen, S. H. Oxide-free Hybrid Silicon Nanowires: From Fundamentals to Applied Nanotechnology. *Prog. Surf. Sci.* **2013**, *88*, 39−60.

(15) Avasthi, S.; Lee, S.; Loo, Y.-L.; Sturm, J. C. Role of Majority and Minority Carrier Barriers Silicon/Organic Hybrid Heterojunction Solar Cells. *Adv. Mater.* **2011**, *23*, 5762−5766.

(16) Fute, Z.; Tao, S.; Baoquan, S. Conjugated Polymer−Silicon Nanowire Array Hybrid Schottky Diode for Solar Cell Application. *Nanotechnology* **2012**, *23*, 194006.

(17) Zhang, J.; Zhang, Y.; Zhang, F.; Sun, B. Electrical Characterization of Inorganic−Organic Hybrid Photovoltaic Devices Based on Silicon-Poly(3,4-ethylenedioxythiophene):poly(styrenesulfonate). *Appl. Phys. Lett.* **2013**, *102*, 013501.

(18) Thiyagu, S.; Hsueh, C.-C.; Liu, C.-T.; Syu, H.-J.; Lin, T.-C.; Lin, C.-F. Hybrid Organic−Inorganic Heterojunction Solar Cells with 12% Efficiency by Utilizing Flexible Film-Silicon with a Hierarchical Surface. *Nanoscale* **2014**, *6*, 3361−3366.

(19) Shrotriya, V.; Li, G.; Yao, Y.; Chu, C.-W.; Yang, Y. Transition Metal Oxides as the Buffer Layer for Polymer Photovoltaic Cells. *Appl. Phys. Lett.* **2006**, *88*, 073508.

(20) Ozdemir, B.; Kulakci, M.; Turan, R.; Emrah Unalan, H. Silicon Nanowire-poly(3,4-ethylenedioxythiophene)−poly(styrenesulfonate) Heterojunction Solar Cells. *Appl. Phys. Lett.* **2011**, *99*, 113510.

(21) Schmidt, J.; Titova, V.; Zielke, D. Organic-Silicon Heterojunction Solar Cells: Open-Circuit Voltage Potential and Stability. *Appl. Phys. Lett.* **2013**, *103*, 183901.

(22) Sze, S. M. pn Junction. *Semiconductor Devices:Physics and Technology*, 2nd ed.; John Wiley & Sons, Inc.: Nouméa, New Caledonia, 1985; Chapter 4.

(23) Hunger, R.; Fritsche, R.; Jaeckel, B.; Jaegermann, W.; Webb, L. J.; Lewis, N. S. Chemical and Electronic Characterization of Methyl-terminated Si(111) Surfaces by High-resolution Synchrotron Photoelectron Spectroscopy. *Phys. Rev. B* **2005**, *72*, 045317.

(24) Sharma, M.; Pudasaini, P. R.; Ruiz-Zepeda, F.; Elam, D.; Ayon, A. A. Ultrathin, Flexible Organic−Inorganic Hybrid Solar Cells Based on Silicon Nanowires and PEDOT:PSS. *ACS Appl. Mater. Interfaces* **2014**, *6*, 4356−4363.

(25) Kelzenberg, M. D.; Turner-Evans, D. B.; Kayes, B. M.; Filler, M. A.; Putnam, M. C.; Lewis, N. S.; Atwater, H. A. Photovoltaic Measurements in Single-Nanowire Silicon Solar Cells. *Nano Lett.* **2008**, *8*, 710−714.

(26) Na, S.-I.; Wang, G.; Kim, S.-S.; Kim, T.-W.; Oh, S.-H.; Yu, B.-K.; Lee, T.; Kim, D.-Y. Evolution of Nanomorphology and Anisotropic Conductivity in Solvent-modified PEDOT:PSS Films for Polymeric Anodes of Polymer Solar Cells. *J. Mater. Chem.* **2009**, *19*, 9045−9053.

(27) Huang, J.; Miller, P. F.; Wilson, J. S.; de Mello, A. J.; de Mello, J. C.; Bradley, D. D. C. Investigation of the Effects of Doping and Post-Deposition Treatments on the Conductivity, Morphology, and Work Function of Poly(3,4-ethylenedioxythiophene)/Poly(styrene sulfonate) Films. *Adv. Funct. Mater.* **2005**, *15*, 290−296.

(28) Thomas, J. P.; Zhao, L.; McGillivray, D.; Leung, K. T. High-efficiency Hybrid Solar Cells by Nanostructural Modification in PEDOT:PSS with Co-solvent Addition. *J. Mater. Chem. A* **2014**, *2*, 2383−2389.

(29) Peng, K. Q.; Hu, J. J.; Yan, Y. J.; Wu, Y.; Fang, H.; Xu, Y.; Lee, S. T.; Zhu, J. Fabrication of Single-Crystalline Silicon Nanowires by Scratching a Silicon Surface with Catalytic Metal Particles. *Adv. Funct. Mater.* **2006**, *16*, 387−394.

(30) Bansal, A.; Li, X.; Lauermann, I.; Lewis, N. S.; Yi, S. I.; Weinberg, W. H. Alkylation of Si Surfaces Using a Two-Step Halogenation/Grignard Route. *J. Am. Chem. Soc.* **1996**, *118*, 7225−7226.

(31) Kim, Y. H.; Sachse, C.; Machala, M. L.; May, C.; Müller-Meskamp, L.; Leo, K. Highly Conductive PEDOT:PSS Electrode with Optimized Solvent and Thermal Post-Treatment for ITO-Free Organic Solar Cells. *Adv. Funct. Mater.* **2011**, *21*, 1076−1081.

(32) Xie, W. G.; Xu, J. B.; An, J.; Xue, K. Correlation between Molecular Packing and Surface Potential at Vanadyl Phthalocyanine/HOPG Interface. *J. Phys. Chem. C* **2010**, *114*, 19044−19047.

(33) Su, Y. R.; Ouyang, M.; Liu, P. Y.; Luo, Z.; Xie, W. G.; Xu, J. B. Insights into the Interfacial Properties of Low-Voltage CuPc Field-Effect Transistor. *ACS Appl. Mater. Interfaces* **2013**, *5*, 4960−4965.

(34) Palik, E. D. *Handbook of Optical Constants of Solids*, 1st ed.; Academic Press: Boston, MA, 1985.